Structures of small bismuth cluster cations

Rebecca Kelting, Alexander Baldes, Ulrike Schwarz, Thomas Rapps, Detlef Schooss et al.

Citation: J. Chem. Phys. **136**, 154309 (2012); doi: 10.1063/1.3703014
View online: http://dx.doi.org/10.1063/1.3703014
View Table of Contents: http://jcp.aip.org/resource/1/JCPSA6/v136/i15
Published by the American Institute of Physics.

Structures of small bismuth cluster cations

Rebecca Kelting,[1] Alexander Baldes,[1] Ulrike Schwarz,[1] Thomas Rapps,[2] Detlef Schooss,[1,2] Patrick Weis,[1] Christian Neiss,[3] Florian Weigend,[1] and Manfred M. Kappes[1,2]

[1]*Institut für Physikalische Chemie, Karlsruher Institut für Technologie, Fritz-Haber-Weg 2, 76131 Karlsruhe, Germany*

[2] *Institut für Nanotechnologie, Karlsruher Institut für Technologie, Postfach 3640, 76021 Karlsruhe, Germany*

[3]*Lehrstuhl für Theoretische Chemie, Universität Erlangen-Nürnberg, Egerlandstr. 3, 91058 Erlangen, Germany*

(Received 5 March 2012; accepted 28 March 2012; published online 20 April 2012)

The structures of bismuth cluster cations in the range between 4 and 14 atoms have been assigned by a combination of gas phase ion mobility and trapped ion electron diffraction measurements together with density functional theory calculations. We find that above 8 atoms the clusters adopt prolate structures with coordination numbers between 3 and 4 and highly directional bonds. These open structures are more like those seen for clusters of semiconducting-in-bulk elements (such as silicon) rather than resembling the compact structures typical for clusters of metallic-in-bulk elements. An accurate description of bismuth clusters at the level of density functional theory, in particular of fragmentation pathways and dissociation energetics, requires taking spin-orbit coupling into account. For n = 11 we infer that low energy isomers can have fragmentation thresholds comparable to their structural interconversion barriers. This gives rise to experimental isomer distributions which are dependent on formation and annealing histories. © *2012 American Institute of Physics*. [http://dx.doi.org/10.1063/1.3703014]

I. INTRODUCTION

Group-V elements show huge variability in their electrical, mechanical, and thermal properties – ranging from gaseous nitrogen to solid and brittle bismuth. Within the group-V elements, bismuth is the only metal while arsenic and antimony are classed as semi-metals.[1] Under ambient conditions the most stable crystalline form of both bismuth and its lighter group V congeners is a rhombohedral layered structure (α-As, α-Sb, α-Bi) with each atom surrounded by three nearest neighbors within the layer and three atoms at a larger distance in the adjacent layers. In α-Bi, these intra- and inter-layer distances differ by only 15% approaching the simple cubic structure with a coordination number of six. Furthermore, unlike P_4 (white phosphorous) and As_4 (yellow arsenic) a solid Bi_4 form is unknown.[1] In molten salts, however, the heaviest group-V element forms many homopolyatomic ions: Bi_5^{3+} and Bi_8^{2+} are for instance well known as classical examples of electron-deficient polyhedra which follow Wade's Rules of electron-counting.[2,3]

The investigation of bismuth clusters in gas phase dates back to the 1980s.[4–7] Mass spectra of Bi_n^+ produced by laser vaporization showed that singly charged cations with n = 3, 5, and 7 are particularly stable, which is also consistent with Wade's Rules.[5] In addition, photofragmentation patterns have been analyzed[6] for Bi_n^+, n < 8. This revealed that for cluster ions up to 5 atoms two neutral atoms are preferentially lost, whereas Bi_6^+ and Bi_7^+ fragment by loss of three atoms. Only for Bi_8^+, was the loss of four atoms (presumably a neutral tetramer) found to be the most prominent fragmentation pathway. This switch of dominant fragmentation channel at eight atoms has been confirmed by the collision induced dissociation (CID) studies of Ross *et al.*[7] who have also shown that all Bi_n^+ (8 < n < 15) dissociate via loss of Bi_4 or Bi_{n-4}^+ fragments. The only exception is Bi_{10}^+, where a neutral dimer is preferentially lost instead. In the latter study, the smaller clusters (n < 8) were observed to preferentially fragment into odd-numbered cluster ions – typically via loss of one atom in the case of even numbered parents or two atoms in the case of odd clusters. Loss of dimer and tetramer units from energized Bi_n^+ (n = 3-8) has also been observed in the surface-induced-dissociation (SID) measurements of Bernhardt *et al.*[8] Neutral bismuth clusters have been investigated in a Stern-Gerlach experiment by Yin *et al.*[9] and the magnetic moments have been determined for Bi_n ($2 \leq n \leq 13$). These show paramagnetic behaviour for odd numbered clusters whereas even numbered clusters showed no response. Anionic bismuth clusters have been studied by means of photoelectron spectroscopy[10–12]: By comparison with density functional theory (DFT) calculations it has been shown that Bi_5^- is aromatic and forms a planar ring.[11–14] More recently, larger neutral and charged bismuth clusters have been the focus of several theoretical studies.[15–17] Yuan *et al.* have calculated structures, fragmentation behavior, and magnetic moments for bismuth clusters up to 24 atoms using density-functional theory. They find that clusters in this size range "prefer semiconducting character" and that particularly the largest species studied have a tendency to form "amorphous structures".[17]

So far, the structure of isolated bismuth clusters has not been directly probed by experiment. The aim of the present article is therefore to establish equilibrium structures for positively charged bismuth clusters of up to 14 atoms via

a combination of ion mobility spectrometry and trapped ion electron diffraction measurements. We compare the experimental data with candidate structures resulting from a systematic search for low-energy structural isomers using two-component density functional theory based on a genetic algorithm. Specifically, a comparison of experiment with the cross sections and modified molecular scattering functions obtained for the calculated structures allows us to confirm or rule out the predictions from theory – thus enabling unequivocal structural assignment for most cluster sizes.

II. EXPERIMENT

A. Ion mobility spectrometry

The experimental setup has been described in detail elsewhere.[18] Bismuth cluster ions are produced in a modified Smalley-type laser vaporization source[19–21] with a rotating target consisting of pressed bismuth powder (99.9% Chempur) and a pulsed valve (General Valve Corp.) providing the cooling gas (He, backing pressure 5 bar). The source is held at room temperature. For vaporization the second harmonic (532 nm) of a Nd-YAG laser (Continuum-ND61) is focused through a 1 mm diameter, 90° conical nozzle onto the target. The resulting cluster beam enters the acceleration region of a linear time-of-flight mass spectrometer and the cluster ions are extracted via a pulsed extraction field (4.5 kV acceleration voltage). The corresponding mass spectrum is monitored with an auxiliary detector, which can be moved into the cluster ion beam prior to the drift cell. The cluster sizes of interest are isolated using a pulsed electrostatic mass gate in front of the cell. The mass selected ion packet is then decelerated (to typically 350 eV kinetic energy, lab frame) to reduce fragmentation – see below. After being focused by an RF-ion funnel, the ions are injected through a 0.5 mm aperture into a 140 mm long variable temperature drift cell, filled with 7 mbar of helium. Inside the cell the ions are guided by a weak electric field (10-30 V/cm) towards the 0.5 mm exit aperture at the end of another ion funnel. A quadrupole mass filter (Extrel C50, up to 4000 amu) behind the drift cell removes (or selects, see below) fragmentation products. The ion arrival time is monitored as a function of the applied drift voltage (pressure and temperature within the cell are kept constant) allowing to determine the mobility and thus the collision cross section of an ion. This is directly related to the geometry of the cluster ion. The experimental error in the cross section is ±1.5%. For all of the bismuth clusters of interest here, ion arrival time distributions (ATD) were determined both at room temperature (~300 K) and at low temperature (90–150 K). Within the error of the experiment and for a given cluster size, we observed no qualitative differences between the low and room temperature ATDs (i.e., no indication of dramatic temperature dependent changes in isomer composition over the corresponding temperature range).[22] Except for Bi_9^+, which showed a broadened ATD (see below), all other measurements were consistent with the presence in the drift cell of either (i) a single isomer or (ii) of an isomer mixture comprising dominantly species having collision cross sections well within the experimental error (see also supplementary material S10-S12, Ref. 23).

Structural assignment is accomplished by comparison of experimental cross sections with quantum-chemically calculated structure candidates. This procedure requires cross section calculations for these structures. Here the "scattering on electron density isosurface" (SEDI) (Ref. 24) model has been used, where the collision cross section is calculated on the basis of the electron density distribution of each cluster. The SEDI model requires the electron density threshold as adjustable parameter which has to be calibrated against the experimental cross section for one cluster size. Bi_5^+ is used as calibration point, since there is no doubt about the global minimum structure, see below. Note that since the SEDI model explicitly takes only the repulsive interaction between cluster ions and helium atoms into account, it is more accurate at higher temperatures. An attraction due to charge-induced dipole interaction can be ignored – at least at elevated temperatures – due to the very small polarizability of helium. At very low temperatures on the other hand, the mobility of an ion becomes independent of its shape and size and approaches the Langevin limit (the mobility of a point charge in a polarizable gas). Another issue is that for precise cross section measurements it is necessary to keep the temperature constant to within 0.1 K for at least 30 min, this is achieved more easily at room temperature. Therefore we use the room temperature data for cross section determination and comparison with theory.

B. Trapped ion electron diffraction

The details of the trapped ion electron diffraction experiment and the data analysis have been described elsewhere,[25] here only a brief overview will be given. 10^5–10^6 bismuth cluster cations, generated in a magnetron sputter source,[26] are mass-selected to a single cluster size, stored in a radio frequency quadrupole ion trap and thermalized through collisions with He buffer gas to a temperature of 95 ± 5 K. The ion cloud is irradiated by an electron beam (40 keV, ~2–3 μA) from a long focal length electron gun. Diffracted electrons from the clusters are detected by a phosphor screen assembly and integrated on an external CCD camera. A reference picture is accumulated by repeating the sequence without cluster ions in the trap. Roughly 500 pictures are taken leading to a total measurement time of 14–16 h (depending in detail on cluster size; note that n = 10 was the smallest cluster for which TIED measurements were still viable). The summed and reference corrected diffraction pictures are centered and radially averaged, yielding the total experimental scattering intensity, I^{tot}, as a function of the electron momentum transfer, $s = 4\pi/\lambda \sin(\theta/2)$. Considering the atomic scattering intensity, I^{at}, and an additional unspecific flat background, I^{back}, the experimental modified molecular scattering function is calculated as $sM^{expt} = s[(I^{tot} - I^{at} - I^{back})/I^{at}]$. The theoretical modified molecular scattering function is approximated by

$$sM^{theo} = S_c/N \exp\left(-L^2 s'^2/2\right) \sum_{i \neq j}^{N} \sin(r_{ij}s')/r_{ij},$$

where $s' = k_s\ s$, N is the number of atoms in the cluster, S_c and k_s are scaling factors, and r_{ij} is the distance between two atoms in the cluster. L^2 is the mean squared vibrational amplitude averaged over all distances in the cluster and accounts for thermal vibrations. The comparison of the experimental and the theoretical data is done using a χ^2 –fit minimizing the differences by variation of S_c, L, k_s, and parameters of the background function I^{back}. The agreement between experimental scattering function and simulated scattering function of the model structure is measured by a weighted profile factor

$$R_w = \sqrt{\sum_i w_i \left(sM_i^{theo} - sM_i^{expt}\right)^2} \Big/ \sqrt{\sum_i w_i \left(sM_i^{expt}\right)^2},$$

where the weighting factors w_i are calculated from the (error-propagated) standard deviation of the experimental data. Note that because of this dependence comparison of different R_w values (obtained for different trial structures) are only meaningful within a single experimental dataset.

C. Collision induced dissociation

Collision induced dissociation (CID) studies were carried out using the apparatus described under Sec. II A. The procedure to obtain CID mass spectra differs from that used for IMS in two aspects: first, the injection energy was increased to 400 eV in order to induce sufficient fragmentation. Second, the quadrupole mass spectrometer behind the drift cell was scanned across the complete mass range corresponding to parent and fragment ions – versus ion arrival time. The fragmentation mass spectra represented here then correspond to integrals over the complete arrival time distributions of the respective fragments.

III. QUANTUM CHEMICAL CALCULATIONS

Density functional theory molecular electronic structure calculations have been carried out with the program system TURBOMOLE[27] to determine structures and properties of small Bi_n^+-Clusters ($n \leq 14$). For all treatments the Tao, Perdew, Staroverov, Scuseria (TPSS) functional[28] was combined with the resolution of the identity approximation[29] for the Coulomb integrals. The inner 60 electrons were modeled by Dirac-Fock effective core potentials[30] that allow for the inclusion of spin-orbit coupling (SOC) when used within a two-component self-consistent field procedure.[31]

For determining the ground state structures a three step process has been followed.

a. In the first step, we employed a genetic algorithm (GA)[32] for finding the structures lowest in energy. These calculations were carried out with the one-component, scalar-relativistic (i.e., neglecting SOC) approach using the def2-SVP[33] basis set.
b. Afterwards the point group symmetry for each structure of the final population of the GA was determined. The structure parameters were reoptimized using the larger dhf-TZVP-2c basis set[34] at the one-component level. By a vibrational analysis we ensured that we only observed minimum structures and no saddle points.
c. In the last step we reoptimized the structures of step (b) by performing two-component calculations including SOC using the same basis set (dhf-TZVP-2c).

We note in advance that – unlike for example Pb clusters[35] – SOC has significant impact on the results and that results accounting for SOC generally are better in line with the experimental data. We further note that for some cases two-component calculations starting from two different minima of the one-component treatment end up with the same minimum structure. For instance, at the one-component level a tetragonal pyramid corresponds to the global minimum structure of Bi_5^+ whereas a distorted tetragonal pyramidal (one edge is elongated) structure is a higher-lying local minimum (+1.53 eV). A two-component optimization starting there ends up with the undistorted tetragonal pyramid.

In Table I and Figure 1 all isomers with energies less than 0.2 eV above the most stable isomer are listed. This threshold was chosen to be slightly higher than in previous analogous treatments of other elements[35] to be on the safe side – given the unexpectedly large effects observed upon accounting for SOC. The cross sections calculated by the SEDI model were determined as described previously and are listed in Table I. The criteria employed for assignment of a candidate structure to the IMS measurement were: (i) match of the computed cross section (to within 1.5%) and (ii) low relative energy (to within 0.2 eV of the computed ground state).

IV. RESULTS AND DISCUSSION

A. Structures

We have measured the collision cross sections for cationic bismuth clusters in the range between 4 and 14 atoms. Geometries were assigned for each cluster size via comparison with the cross sections for the energetically favorable DFT-optimized structures. For the clusters with 10 to 14 atoms, TIED measurements were also conducted and used for further verification.

IMS calibration: We start our discussion with Bi_5^+, since we used it as the calibration point for the SEDI electron density threshold. The global minimum structure (GM) of Bi_5^+ (5-I) corresponds to a square pyramidal geometry (see Fig. 1) as has been predicted by Yuan *et al.*[17] There is no doubt about the structure of the pentamer since the next higher-lying isomer, a trigonal bipyramid (5-II), is more than 0.5 eV above the GM. The ring (5-III), the favored anionic structure, is 1.6 eV above the GM as the cation. Based on the structure (5-I), we therefore adjust the density threshold of bismuth to 0.0172 $Å^{-3}$ so that the calculated cross section matches the experimental value of 67.4 $Å^2$ – and use this density threshold for all further cluster sizes.

Bi_4^+: For Bi_4^+ the GM is a tetrahedron (4-I) with D_{2d} symmetry (cf.[17]). This can be confirmed by experiment (59.6 $Å^2$ and 59.1 $Å^2$, respectively, see Table I and Figure 2). The tetrahedron is the only stable structure that we find for this cluster size.

TABLE I. Relative energies, collision cross sections, average bond lengths, and coordination numbers for different cluster sizes and isomeric structures. The different isomers are numbered according to Figure 1. The experimental error in cross sections was ±1.5% for all species except for Bi_9^+. Here the presence of a two component isomer mixture led to an only partially resolved ATD and an uncertainty in each cross section of ±2.5%.

Cluster size	Isomer	Point group	$\Delta E_{SO,TPSS}$ (eV)	Ω_{SEDI} (Å^2)	Ω_{exp} (Å^2)	Average bond length (pm)	Average coordination number
4	4-I	D_{2d}	0	59.6	59.1	306.1	3.00
5	5-I	C_{4v}	0	67.4	67.4	307.1	3.20
	5-II	D_{3h}	0.51	67.3		311.8	3.60
	5-II	C_s	1.6	72.3		294.0	2.00
6	6-I	C_2	0	75.0	75.7	312.0	3.33
	6-II	C_s	0.02	75.9		312.6	3.33
	6-III	C_{2v}	0.04	77.4		307.5	3.00
	6-IV	C_2	0.09	77.8		301.6	2.67
7	7-I	C_s	0	82.0	82.0	306.1	3.14
	7-II	C_{3v}	0.54	80.9		311.8	3.43
8	8-I	D_{4d}	0	86.1	86.8	316.9	4.00
	8-II	C_s	0.14	89.0		309.2	3.25
9	9-I	C_{3v}	0	95.5	97.8, 100.8	308.4	3.33
	9-II	C_s	0.18	94.4		310.6	3.33
	9-III	C_{3h}	0.23	96.7		311.0	3.33
	9-IV	C_s	0.27	100.6		309.5	3.33
10	10-I	C_{2v}	0	99.7	101.8	318.3	3.80
	10-II	C_s	0.16	102.0		307.8	3.20
11	11-I	C_2	0	107.6	108.5	305.3	3.09
	11-II	C_s	0.12	117.8		311.3	3.27
12	12-I	C_s	0	115.8	116.6	307.0	3.17
	12-II	C_s	0.03	115.2		306.7	3.17
13	13-I	C_s	0	119.4	121.6	312.5	3.54
	13-II	C_1	0.04	120.8		312.2	3.38
	13-III	C_1	0.07	119.2		311.9	3.38
	13-IV	C_1	0.08	120.9		309.7	3.62
14	14-I	C_1	0	126.8	128.7	306.3	3.14
	14-II	C_s	0	129.6		306.8	3.14
	14-III	C_s	0.25	125.7		305.0	3.00

Bi_6^+: For Bi_6^+ we find three quasi-degenerate structures within 0.04 eV: the energetically lowest one (6-I) can be looked upon as a distorted trigonal anti-prism (C_2 symmetry). Its cross section of 75.0 Å^2 is 1.3% below the experimental value of 75.7 Å^2, close to the error limit of 1.5%. The next isomer (6-II), a capped tetragonal pyramid with C_s symmetry, is only 0.02 eV higher in energy and has a cross section of 75.9 Å^2 that is in agreement with the experimental value as well. Hence, in this case our experiment cannot distinguish between the two structures lowest in energy. Based on the cross section we can however rule out two other structures that are within 0.1 eV of the GM: isomer 6-III (+0.04 eV, 77.4 Å^2), which can be regarded as a capped trigonal bipyramid and isomer 6-IV (+0.09 eV, 77.8 Å^2), a structure based on a pentagonal ring.

Bi_7^+: For the heptamer the GM structure (7-I) is well separated (> 0.5 eV) from all higher lying forms. It can be looked upon as a capped trigonal prism. Six of the constituting atoms are three-fold coordinated, only one is four-fold coordinated. The cross section of 82.0 Å^2 agrees almost exactly with the experimental value (82.0 Å^2). The next isomer (7-II, +0.54 eV) has a cross section (80.9 Å^2) 1.4% below the experimental value, i.e., close to the error limit. Based on the large energy difference to 7-I we rule out this structure. As already mentioned, the results found for this cluster size underscore the importance of including SOC in the calculations: without SOC the GM structure 7-I is calculated to be 0.11 eV *above* 7-II !

Bi_8^+: For the GM (8-I) we find a tetragonal antiprism (D_{4d} symmetry). This structure is rather unusual in as much as all eight atoms are four-fold coordinated – as a general rule we observe a large number of three-fold coordinated atoms in the majority of cluster sizes studied here. Nevertheless, we can confirm this structure: its cross section (86.1 Å^2) agrees to within 0.8% with the experimental value (86.8 Å^2) .The next isomer 8-II (0.14 eV), which is the structure favored by Yuan *et al.*,[17] can be ruled out based on its larger cross section of 89.0 Å^2 which is 2.5% above the experimental value. Note again the large influence of SOC: without SOC 8-II is predicted to be the GM, being 0.03 eV lower than 8-I.

Bi_9^+: From the experimental point of view the nonamer is a special case: we observe an arrival time distribution

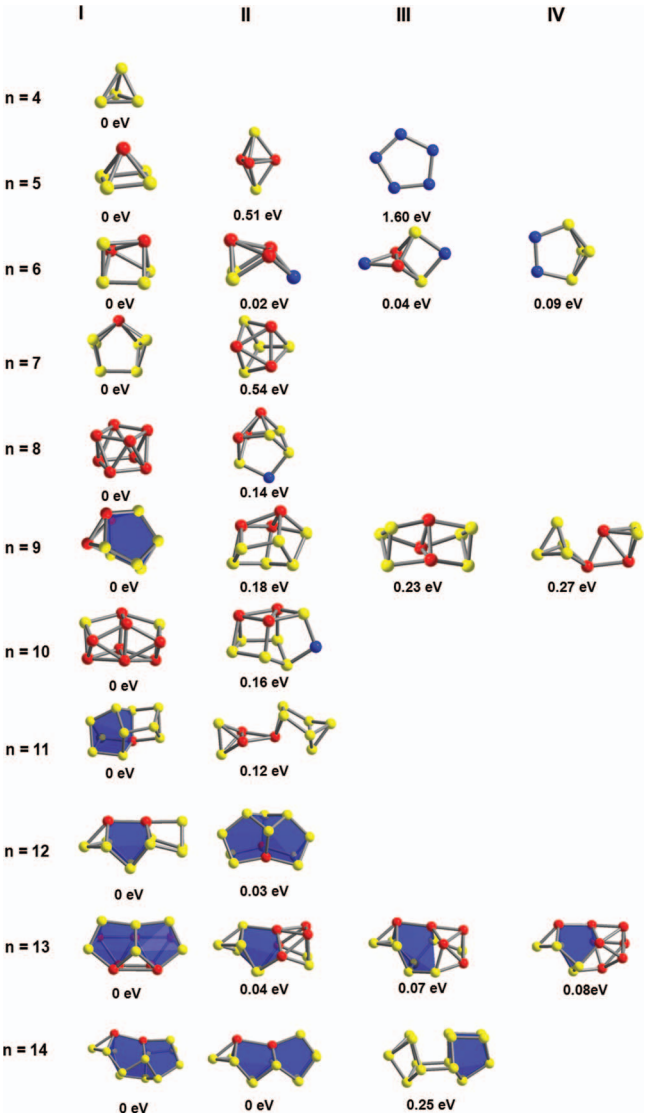

FIG. 1. Calculated local minimum structures for Bi_4^+–Bi_{14}^+. All geometries are optimized at the DFT-TPSS level. The figures in column I correspond to the respective global minima (GM). In the main text, we refer to the structures/isomers in terms of a short hand nomenclature, x-y, where x corresponds to the cluster size and y to the isomer number (Roman numerals) as shown in this figure. Atoms are labeled according to their coordination number (2 = blue, 3 = yellow, ≥4 = red). The corresponding coordinates (as xyz-files) are available as supplementary material S9.[23]

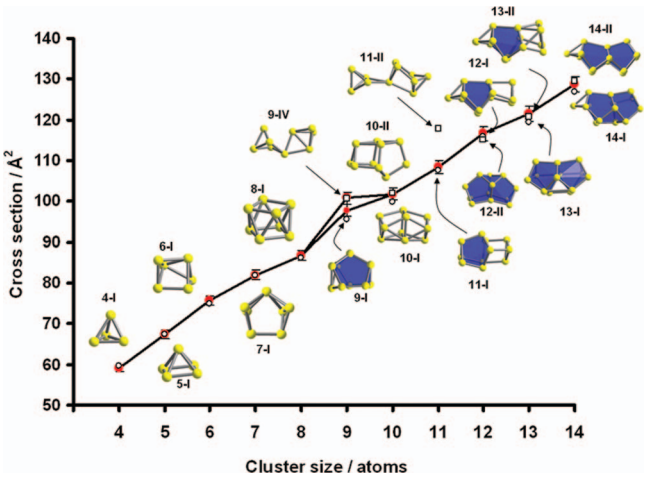

FIG. 2. Collision cross sections of bismuth cluster cations as a function of cluster size. Experimental values are shown as full circles together with corresponding error bars. Theoretical global minimum structures are shown as open circles, other relevant isomers (see text for details) are shown as open squares. Cross sections were calculated with the SEDI-model using the coordinates from DFT calculations.

that is significantly broader than what we find for the other cluster sizes (where the peak width corresponds to our experimental resolution), see Figure 3. We can identify at least two partially overlapping peaks, i.e., at least two different isomers are present that do not interconvert on the timescale of drift cell passage (1 ms). To explain the ATD these isomers must differ in cross section by roughly 3%, corresponding to 97.8 Å^2 vs. 100.8 Å^2. Based on the difficulty to identify the exact peak positions from an only partially resolved ATD we have to accept an uncertainty in the cross section of 2.5% instead of the usual 1.5% for the other cluster sizes. The GM we find (9-I) has a cross section of 95.5 Å^2, corresponding to the first peak in our arrival time distribution. The next isomer (9-II), the structure favored by Yuan *et al.*,[17] is 0.18 eV higher in energy, has an even smaller cross section (94.4 Å^2), and can therefore be ruled out. The question as to what structure corresponds to the second, roughly equiabundant isomer remains open at this writing: 9-IV, the only structure that agrees well with the experimental cross section (100.6 Å^2 vs. 100.8 Å^2) is 0.27 eV higher in energy than the GM. The GM structure itself deserves closer inspection: it consists of eight atoms arranged

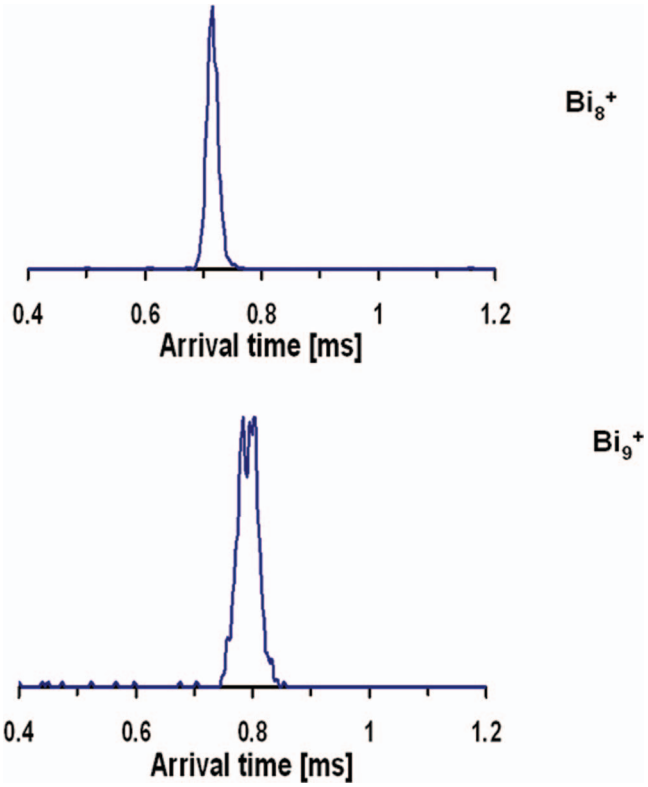

FIG. 3. Typical arrival time distributions (ATD) for Bi_8^+ and Bi_9^+. The width of the Bi_8^+–ATD (and of all Bi_n^+ except n = 9) corresponds to our instrumental resolution – see also supplementary material S10-S12.[23] Note that the Bi_9^+-ATD is significantly broader and bimodal indicating the presence of (at least) two isomers.

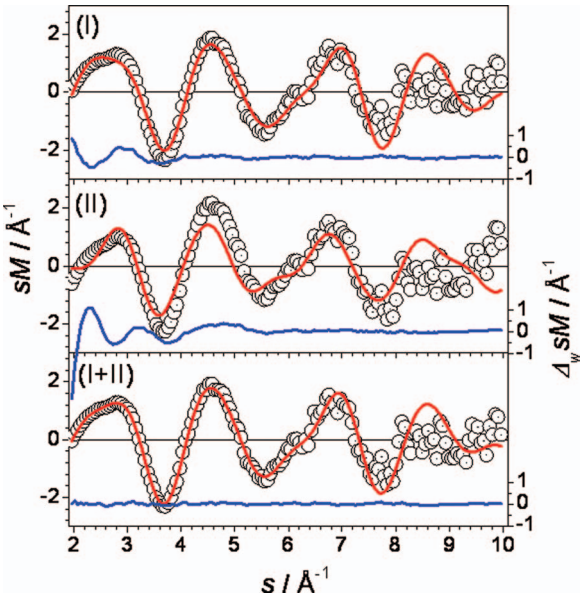

FIG. 4. Comparison of modified experimental (open circles) and theoretical (red lines) molecular scattering functions *sM* for Bi_{10}^+ isomers 10-I (R_w = 14%) and 10-II (R_w = 44%) as well as for a mixture (0.75:0.25) of both (R_w = 4.5%). The lower traces show the weighted residuals (blue lines).

in two pentagonal rings sharing one edge (see Figure 1, marked as blue polyhedron) plus one capping atom. This motif determines the structure of most of the larger cluster sizes, see below.

Bi_{10}^+: This is the first cluster size, where in addition to the IMS data also TIED measurements are available. In the calculations we find the same GM structure (10-I, 99.7 Å^2) as Yuan *et al.*,[17] a triple-decker consisting of a central planar four-membered ring (C_{2v} symmetry). This structure is 2.1% below the experimental cross section value of 101.8 Å^2 and therefore we can rule out that it contributes strongly to the cross section measurement – which shows a typical monoisomeric ion arrival time distribution. In contrast, a structure whose cross section (102.0 Å^2) fits the experimental value almost exactly is found 0.16 eV higher in energy (10-II; again consisting of fused pentagonal rings). The TIED measurement provides further information: fitting each of the structures individually to the low temperature (95 K) scattering data leads to unsatisfactorily large profile factors (14.0% for 10-I and 44% for 10-II, respectively) – i.e., neither of the isomers can by themselves explain the experimental molecular scattering function. However, a significantly lower profile factor (R_w = 4.5%, see Figure 4) is obtained by assuming a two component mixture of 10-I and 10-II (optimum ratio 75:25%, see supplementary material S1[23]) indicating that isomer I is the dominant contributor in the 95 K TIED measurement.

At this stage it is of interest to consider the hypothetical equilibrium ratios of candidate isomers. Assuming I-II isomer interconversion is possible and therefore that equilibrium can be reached in our experiments, a I/II energy difference of 0.16 eV corresponds to isomer II equilibrium compositions of 0.0%, 0.0% and 0.2% at 95, 120, and 300 K, respectively. These predicted compositions are clearly not in agreement with either experiment. A 25% isomer II fraction like that seen in TIED at 95 K is obtained upon assuming a smaller I/II energy difference of 0.006 eV (cf. 31% and 44% at 120 and 300 K, respectively). A roughly equiabundant mixture of isomers I and II should however give rise to an ATD just outside of the error range of the room temperature IMS experiment. Nevertheless it seems to be the most plausible rationalization for both experiments – as long as we adhere to the assumption (consistent with all of our previous metal cluster structure determinations) that we are studying thermodynamically predicated isomer distributions.

Bi_{11}^+: For the GM of Bi_{11}^+ (11-I) we find the same structural motif of two pentagons sharing a common edge as for (9-I). The cross section of this structure (107.6 Å^2) agrees to within 1% with the experimental value of 108.5 Å^2. The next higher lying isomer (+0.12 eV) is a strongly prolate structure (11-II). It has a cross section of 117.8 Å^2, more than 8% above the experimental value. This structure can clearly be ruled out from the IMS experiment, i.e., we only observe the GM structure 11-I at room temperature. This observation does not change upon repeating the IMS measurement at low temperature (120 K): again a dominantly monoisomeric ATD is observed consistent with 11-I.

Interestingly, the low temperature TIED experiment appears to be in *qualitative disagreement* with IMS observations. In order to explain the diffraction data (95 K) for Bi_{11}^+, we need to consider a two component mixture comprising both 11-I and 11-II. Each of the two structures by itself shows unsatisfactorily high R_w values (32.4% for isomer 11-I and 30.2% for isomer 11-II, respectively). However, a mixture of both isomers in a 50:50% ratio results in an optimum R_w value of 5.5% (see supplementary material S2 and S3[23]). Such an equiabundant mixture should give rise to a low temperature ATD with bimodal shape. This is not observed. Agreement with the IMS measurement improves when carrying out TIED on Bi_{11}^+ ions at room temperature: now only isomer 11-I is found (see supplementary material S4[23]).

These results cannot be explained by simple thermodynamic arguments: i.e., given that the 0 K energies of both isomers are so close (and assuming that their vibrational energy distributions are in fact similar), the free energy difference and corresponding room temperature equilibrium ratio is inconsistent with the absence of one of the two isomers as seen in the TIED measurement. (Note: Based on a II-I energy difference of 0.12 eV we calculate isomer II equilibrium compositions of 0.0%, 0.2%, and 60% at 95, 120, and 300 K, respectively – inconsistent with TIED. A 50% fraction of II is found at 95 K only if the II-I energy difference is very small ($\sim$ +0.04 eV). However, then isomer II is expected to dominate at room temperature (51%, 72%, 96% for 90 K, 120 K, 300 K, respectively) – inconsistent with both TIED and IMS. To get only isomer I at RT, the II-I energy difference has to be $\sim$ 0.25 eV or greater.)

This leads us to the conclusion, that in this case, we apparently do not reach chemical equilibrium. Note that in all comparative IMS and TIED studies performed so far on metal clusters we have observed no indication for metastable species.[36–38] One possible explanation for these findings is that isomer II is lost before the structure dependent

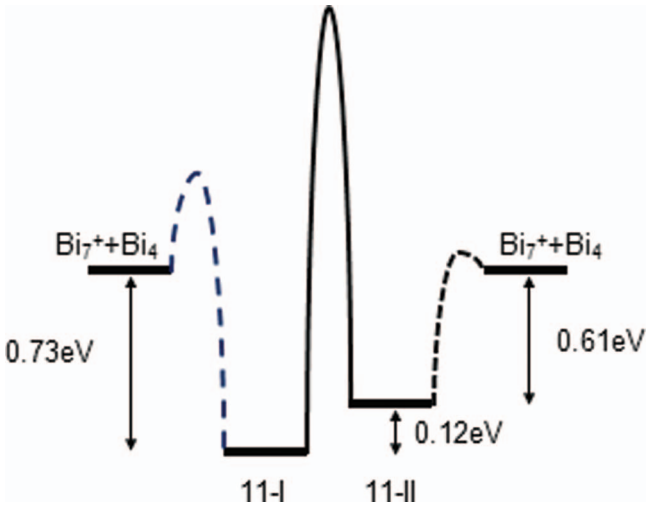

FIG. 5. Schematic energy diagram including inter-conversion and fragmentation barriers for Bi_{11}^+ isomers 11-I and 11-II (see text).

measurement is taken, i.e., during injection into the drift cell in IMS or during trapping in the TIED experiment. In both cases a fraction of the lab frame kinetic energy (~300 eV IMS, ~25 eV TIED) is converted (via collisions with helium) into internal excitation of the cluster. This in turn can lead to a preferential dissociation of one of the isomers if the relative barrier heights for dissociation and inter-conversion were as depicted in Figure 5. Even though the energies of isomer 11-I and 11-II differ by only 0.12 eV, inter-conversion would be hindered by a large energy barrier whereas the fragmentation barrier (leading to Bi_4 and Bi_7^+ for each isomer) might be significantly lower. Additionally, in Isomer 11-II the tetrahedral Bi_4 unit is already essentially preformed. Therefore it seems plausible to assume a smaller, almost barrier-less fragmentation route for isomer 11-II, so that it dissociates preferentially if the internal energy reaches the necessary threshold. This would also explain the significant fragmentation during the injection/trapping process which was observed for both IMS and room temperature TIED measurements. In contrast, in the low temperature TIED measurement (for which no significant fragmentation could be detected) the increase in internal energy induced by trapping collisions would not be sufficient to induce dissociation and consequently a mixture of both isomers can be measured. An alternative explanation would be that in the room temperature TIED and IMS measurements, thermodynamic equilibrium can be established (favoring isomer I, which is according to the DFT calculations lower in energy by 0.12 eV), but that the 25 eV injection energy in the low temperature TIED experiment is not sufficient to overcome the activation barrier for isomerisation. Therefore isomer II might be present as a metastable species.

We note that the present experimental setup does not allow us to distinguish between the proposed kinetic models. It is however clear that the isomerisation barrier between isomer-I and isomer-II is exceptionally high, whether or not it is higher than the dissociation energy remains an open question.

In future it will be of interest to perform appropriate spectroscopic studies to prove the proposed isomer-selective decay (e.g., via IR-MPD).

Bi_{12}^+: For Bi_{12}^+ theory finds two topologically different structures that are almost isoenergetic. Both structures show the same edge-sharing-pentagon-motif: the lowest energy structure 12-I can be looked upon as nonamer-GM 9-I (edge-sharing-pentagons plus capping atom) with a Bi_3-ring attached (see Figure 1). Its cross section of 115.8 Å^2 agrees within 0.7% with experiment. Only 0.03 eV higher in energy is a structure (12-II) that comprises two fused edge-sharing-pentagonal units. The cross section of 115.2 Å^2 is still within the IMS error limit, i.e., we cannot distinguish between the two isomers on basis of IMS alone. However, in the TIED measurement (see supplementary material S5[23]) a significantly larger profile factor ($R_w = 17.1\%$) is found for isomer 12-I, whereas a profile factor of 6.3% is found for structure 12-II. A mixture of both does not lead to an improved agreement suggesting that structure 12-II is the dominant isomer formed for Bi_{12}^+.

Bi_{13}^+: As for Bi_{12}^+ we find two topologically different structures based on edge-sharing pentagons which are very close in energy: The GM (13-I) is closely related to 12-II (see Figure 1), while 13-II (+0.04 eV) can be looked upon as 12-I with the Bi_3-ring replaced by a planar Bi_4-ring. 13-I has a cross section of 119.4 Å^2, 1.8% below the experimental value of 121.6 Å^2 while 13-II (120.8 Å^2) is in much better agreement (−0.7%). In TIED we observe a mixture with 13-I as the dominant species: for isomer 13-I a profile factor of 7.01% has been found whereas 13-II has a much larger R_w value of 23.7% (see supplementary material S6[23]). Here a fit of a mixture of both isomers in a 75:25% ratio leads to an optimum profile factor of 3.5%. Additional isomers that are variations of structure 13-II have also been found to lie within 0.1 eV of the GM but do not agree with experimental (TIED) data (see supplementary material S7[23]).

Bi_{14}^+: We find two degenerate structures within 0.01 eV of each other (14-I and 14-II). Both are structurally closely related: two fused edge-sharing pentagonal units plus one capping atom. The main difference between 14-I and 14-II is that the pentagonal units are flipped by 180°. As a result 14-I is slightly more compact (126.8 Å^2, 1.5% below the experimental value of 128.7 Å^2) than 14-II (129.6 Å^2, 0.7% above). Based on the cross section alone we cannot distinguish between these structures. We can however rule out the next-higher-lying isomer: 14-III is 0.25 eV higher in energy, whereas its cross section is 2.3% below experiment. Using the TIED results, however, also allows us to rule out isomer 14-II ($R_w = 12.3\%$). GM 14-I has the lowest profile factor of 5.9%, which cannot be improved by assuming an isomer mixture with one of the other isomers, i.e., the GM appears to be the dominant isomer for Bi_{14}^+(see supplementary material S8[23]).

To summarize, we can confirm a transition from more compact structures at small cluster sizes towards more open, prolate structures ("amorphous-like") at larger sizes as predicted in the DFT calculations of Yuan *et al.*[17] However, we observe differences in structural details which are attributable to the influence of SO-coupling. As a general rule, the

assigned (open) structures are characterized by low atomic coordination numbers – most often three or four (assuming a threshold of 3.5 Å for assigning a bond). In this respect the structures are quite untypical for "metal" clusters. The average bond lengths and coordination numbers (see Table I) show no obvious trend over the size range investigated (n = 4-14): Most low energy structures have average bond length between 305 pm and 313 pm and average coordination numbers between 3 and 3.5. Exceptions are the GM structures of Bi_8^+ and Bi_{10}^+: both have larger coordination numbers (4 and 3.8 respectively) and larger average bond lengths (316.9 pm and 318.3 pm respectively). In bulk bismuth each atom is threefold coordinated with a distance of 307.2 pm to its nearest neighbors (further there are three next-nearest neighbors at a distance of 352.9 pm),[39] i.e., for most cluster sizes we observe bond parameters close to the bulk values.

B. Fragmentation patterns and fragmentation energies

The fragmentation patterns are dominated from n = 8 to n = 14 by the loss of a neutral Bi_4 (presumably a GM tetrahedron), while dimer or monomer loss is favored for the smaller clusters, see Figure 6 and Table II. When comparing the experimental fragment intensities with the DFT-computed fragmentation energies for the lowest energy channels, we observe a nearly perfect correlation (Table II). In the case of Bi_{10}^+, for example, we observe three dominant fragmentation channels (dimer, trimer, and tetramer loss with relative intensities of 11%, 13%, and 54%, respectively). Their occurrence and their relative intensities are quite well reflected by the close-lying (lowest) dissociation energies predicted from calculations (1.57 eV, 1.52 eV, and 1.41 eV, see Table II). We note, that a high quality correlation between experiment and theory results only from inclusion of spin-orbit interactions in the calculations. Within the scalar-relativistic approach, tetramer loss is favored as well, but trimer/dimer loss is calculated to be 0.68/1.03 eV higher in energy. For the fragmentation of Bi_5^+ the situation is even more extreme. Without spin-orbit interaction, monomer loss is favored and the experimentally observed dimer loss would lie 0.28 eV higher in energy (and would therefore not be expected). By including spin-orbit interaction, monomer and dimer loss are predicted to have nearly the same threshold energies. In the fragmentation mass spectra taken at 400 eV injection energy (see Figure 6) a significant part of the parent Bi_n^+ (n = 4, 5, 6, 7, 8, 10) remains intact, whereas for Bi_n^+ (n = 9, 11, 12, 13, 14) nearly complete decay can be observed. The calculated

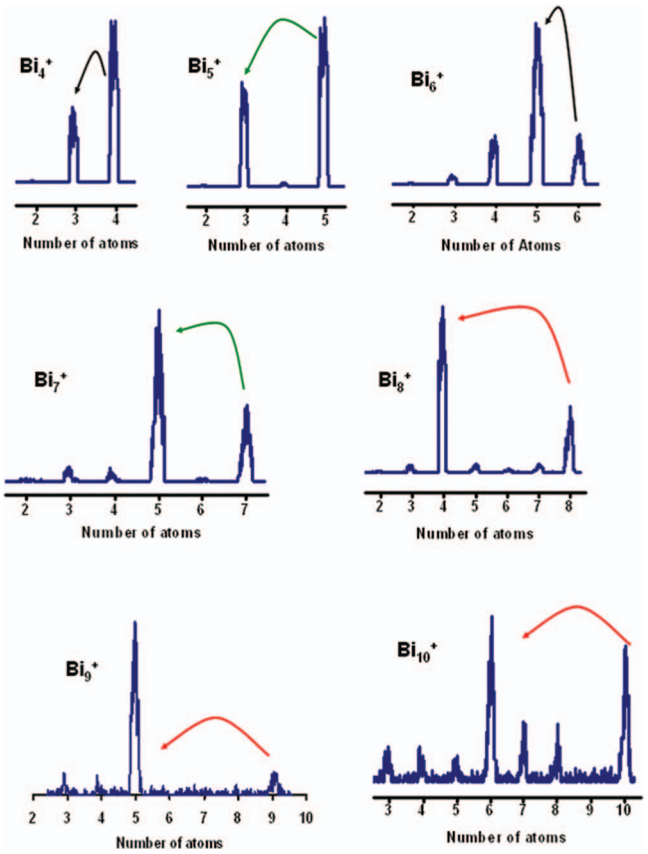

FIG. 6. Typical fragment. ion mass spectra obtained at a collision energy of 400 eV (lab frame). The corresponding Bi_x^+ parent ions were as indicated.

TABLE II. Fragmentation pattern of bismuth cluster cations. The first column lists the parent cluster ions. These fragment into the cations given in the appropriate rows together with a corresponding neutral cluster. In each cell of the table the upper value is the fragmentation energy calculated as the total energy difference (eV) of the parent and the sum of the neutral and the cationic fragment; the lower value in brackets is the experimentally measured relative intensity (%) of that particular fragment. The relevant experimental parameters are helium pressure in the drift cell of 6 mbar and injection energy of the ions 400 eV (lab-frame). Relative intensities above 10% and fragmentation energies within 0.2 eV of the lowest energy channel are shown in bold print.

	Fragment											
Parent	Bi_{13}^+	Bi_{12}^+	Bi_{11}^+	Bi_{10}^+	Bi_9^+	Bi_8^+	Bi_7^+	Bi_6^+	Bi_5^+	Bi_4^+	Bi_3^+	Bi_2^+
Bi_{14}^+	1.84 (< 2)	1.74 (< 2)	1.63 (< 2)	**0.83 (37)**	1.63 (< 2)	(2)	(2)	**(33)**	(7)	(8)	**(11)**	(< 2)
Bi_{13}^+	…	2.13 (< 2)	1.57 (< 2)	1.85 (< 2)	**0.85 (47)**	1.74 (< 2)	(5)	(< 2)	**(34)**	(4)	(8)	(< 2)
Bi_{12}^+	…	…	1.66 (< 2)	1.49 (< 2)	1.57 (< 2)	**0.66 (74)**	1.34 (4)	(2)	(5)	(8)	(6)	(< 2)
Bi_{11}^+	…	…	…	2.06 (< 2)	1.68 (< 2)	1.85 (< 2)	**0.73 (83)**	2.41 (< 2)	(6)	(4)	(7)	(< 2)
Bi_{10}^+	…	…	…	…	1.85 (< 2)	**1.57 (11)**	**1.52 (13)**	**1.41 (54)**	1.72 (6)	(8)	(8)	(< 2)
Bi_9^+	…	…	…	…	…	1.95 (< 2)	1.45 (< 2)	2.41 (< 2)	**0.92 (90)**	2.25 (4)	(6)	(< 2)
Bi_8^+	…	…	…	…	…	…	1.73 (5)	2.24 (< 2)	1.82 (4)	**1.36 (86)**	2.57 (6)	(< 2)
Bi_7^+	…	…	…	…	…	…	…	2.73 (< 2)	**1.87 (89)**	2.48 (4)	**1.89 (6)**	3.74 (< 2)
Bi_6^+	…	…	…	…	…	…	…	…	**1.36 (78)**	**1.52 (18)**	2.01 (4)	2.06 (< 2)
Bi_5^+	…	…	…	…	…	…	…	…	…	**2.38** (3)	**2.43 (96)**	3.55 (< 2)
Bi_4^+	…	…	…	…	…	…	…	…	…	…	**2.27 (99)**	2.94 (< 2)

fragmentation energies for the latter are 0.92 eV (Bi_9^+) or less, which is apparently low enough to ensure complete fragmentation under the experimental conditions. For the former group, energies are 1.36 eV (Bi_8^+) or above. The stability of these cations is too high to achieve total decomposition.

Bi_{14}^+ and Bi_{13}^+ are cases of special interest because of the high relative intensities of smaller cations such as Bi_6^+ and Bi_5^+ in their fragmentation mass spectra. We interpret this as due to the occurrence of sequential fragmentation reactions as follows:

1. $Bi_{13}^+ \rightarrow Bi_9^+ \rightarrow Bi_5^+ \rightarrow Bi_3^+$
   The first fragmentation step to Bi_9^+ corresponds to an energetically favourable tetramer loss as observed for all larger Bi_n^+ clusters. This process goes nearly to completion and consumes 0.83 eV. In a second step, Bi_9^+ apparently loses a further Bi_4. Again this is energetically favored (0.92 eV). Further fragmentation of the resulting Bi_5^+ is then only a minor channel (also due to the high energy of around 2.4 eV for dimer and monomer loss).
2. $Bi_{14}^+ \rightarrow Bi_{10}^+$
   The first step is again associated with tetramer loss – as for Bi_{13}^+. The resulting Bi_{10}^+ can then fragment along several energetically comparable pathways (see above):
   a. $Bi_{10}^+ \rightarrow Bi_6^+ \rightarrow Bi_5^+ \rightarrow Bi_3^+$
   b. $Bi_{10}^+ \rightarrow Bi_7^+ \rightarrow Bi_5^+ \rightarrow Bi_3^+$
   c. $Bi_{10}^+ \rightarrow Bi_8^+ \rightarrow Bi_4^+ \rightarrow Bi_3^+$
   None of these steps would by themselves lead to significant relative fragment intensities for Bi_3^+. However, in combination they could easily add up to a fragment intensity of >10% as in fact observed.

C. Bond energies per atom

In Figure 7, we display the bond energies per atom of the cluster sizes studied here:

$$BE(Bi_n^+) = [E(Bi^+) + (n-1) * E(Bi) - E(Bi_n^+)]/n$$

and their second order differences:

$$\Delta_2(Bi_n^+) = E(Bi_{n-1}^+) + E(Bi_{n+1}^+) - 2 * E(Bi_n^+).$$

The bond energy per atom (BE) rapidly increases from Bi_2^+ (1.17 eV) to Bi_5^+ (1.98 eV), shows a slight decrease at Bi_6^+ and then increases again to reach its maximum value at Bi_7^+ (2.00 eV). For the larger clusters, BE remains almost constant (1.93–1.96 eV) albeit slightly smaller. We note in passing that in preliminary BE calculations of the larger species Bi_{24}^+ (1.92 eV) we have seen no further increase (the structure was taken from Ref. 17 and reoptimized at two-component level). We note further that in particular for small n, $BE(Bi_n^+)$ is significantly larger than the analogously defined quantity for neutral clusters, $BE(Bi_n)$, simply because of the larger relative contribution of ionization to the thermodynamic sums. For instance, $BE(Bi_7^+)$ amounts to 2.00 eV, whereas $BE(Bi_7^0)$ is 1.68 eV (same topology). For larger cationic systems in contrast, BE values become more similar to those of neutral clusters. Here one can compare to the cohesive energy of the bulk, which is still somewhat higher: 2.15 eV.[40] It

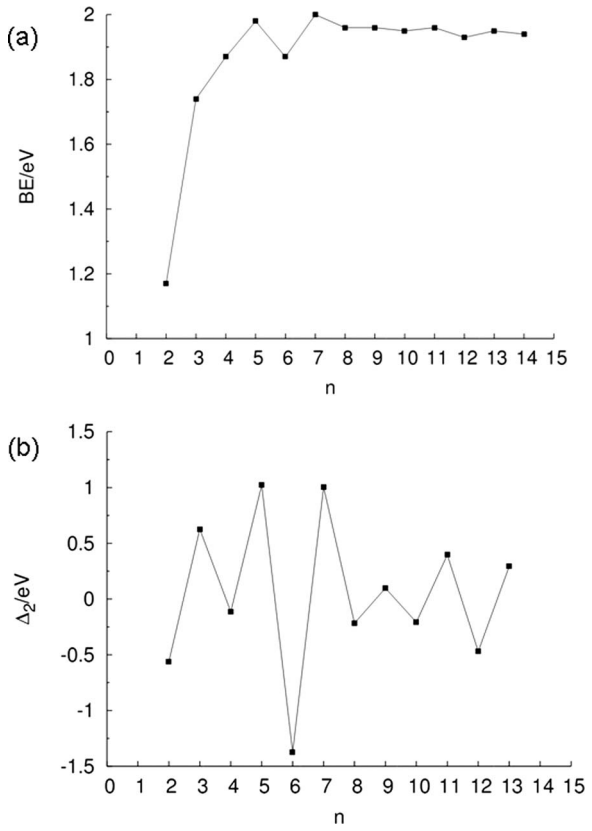

FIG. 7. (a) Calculated bond energies per atom ($BE(Bi_n^+)$), and (b) their second-order differences $\Delta_2(Bi_n^+)$. See text for details.

is likely that the BE values at the plateau reached at ~10 atoms in our study are still somewhat smaller than those for very large clusters for which structure motifs are expected to relate more to the bulk, i.e., higher compactness and thus higher coordination numbers. Neglecting SOC leads to BEs that are ~0.5 eV higher. This can be traced back to the already poor description of the atom (and the atomic cation) without SOC, as has been discussed for Pb and Po.[31] As a consequence, when neglecting SOC one obtains unrealistic cohesive energies *above the bulk value* for rather small clusters of ~20 atoms.[16]

For the second-order energy differences, even-odd oscillations are evident: clusters with odd numbers of atoms, i.e., even number of electrons, are more stable than clusters with even numbers of atoms. Such enhanced relative stability of electronically closed-shell systems has also been observed for the neutral bismuth cluster systems.[16]

V. CONCLUSIONS AND SUMMARY

By combining ion mobility spectrometry, trapped ion electron diffraction, and density functional theory calculations (including spin-orbit coupling) we find that bismuth cluster cations Bi_n^+, $8 < n < 15$, adopt open, prolate structures with low coordination numbers. As a general structural motif we find two pentagons sharing a common edge (wedgelike structure). Therefore at least structurally, such aggregates of bismuth behave more like clusters of semiconducting-in-bulk elements (such as silicon) rather than like the more compact clusters of typical metallic-in-bulk

elements (such as lead). Furthermore we find that for bismuth cluster cations spin-orbit coupling (SOC) has significant influence on the energetic sequence of isomers and in particular on the fragmentation pathways/energetics. In line with previous observations,[41] including SOC leads to preference of higher symmetric isomers, e. g., for Bi_8^+ a D_{4d}-structure is observed with SOC, without it is distorted towards C_2. This cluster system is unusual among those for which we have so far obtained direct structural information from experiment in that certain sizes (e.g., n = 11) are formed as mixtures of low energy isomers which can apparently have fragmentation thresholds which are lower than structural interconversion barriers. This may give rise to experimental isomer distributions determined by fragmentation kinetics rather than equilibrium thermodynamics.

ACKNOWLEDGMENTS

This research was supported by the Deutsche Forschungsgemeinschaft (DFG) as administered by the Karlsruhe Center for Functional Nanostructures (CFN). We are also grateful to the Bundesministerium für Bildung und Forschung (BMBF) through the Helmholtz Research Program POF NanoMikro and to the State of Baden-Württemberg for providing the necessary infrastructure.

[1] N. N. Greenwood and A. Earnshaw, *Chemistry of the Elements*, 2nd Ed. (Elsevier, 1997).
[2] G. Day, R. Glaser, N. Shimomura, A. Takamuku, and K. Ichikawa, Chem. Eur. J. **6**, 1078 (2000).
[3] A. N. Kuznetsov, L. Kloo, M. Lindsjö, J. Rosdahl, and H. Stoll, Chem. Eur. J. **7**, 2821 (2001).
[4] R. G. Wheeler, K. Laihing, W. L. Wilson, and M. A. Duncan, Chem. Phys. Lett. **131**, 1 (1986).
[5] M. E. Geusic, R. R. Freeman, and M. A. Duncan, J. Chem. Phys. **89**, 223 (1988).
[6] M. E. Geusic, R. R. Freeman, and M. A. Duncan, J. Chem. Phys. **88**, 163 (1988).
[7] M. M. Ross and S. W. McElvany, J. Chem. Phys. **89**, 4821 (1988).
[8] T. M. Bernhardt, B. Kaiser, and K. Rademann, Z. Phys. D: At., Mol. Clusters **40**, 327 (1997).
[9] S. Yin, X. Xu, R. Moro, and W. A. de Heer, Phys. Rev. B **72**, 174410 (2005).
[10] M. L. Polak, J. Ho, G. Gerber, and W. C. Lineberger, J. Chem. Phys. **95**, 3053 (1991).
[11] M. Gausa, R. Kaschner, H. O. Lutz, G. Seifert, and K.-H. Meiwes-Broer, Chem. Phys. Lett. **230**, 99 (1994).
[12] M. Gausa, R. Kaschner, G. Seifert, J. H. Faehrmann, H. O. Lutz, and K.-H. Meiwes-Broer, J. Chem. Phys. **104**, 9719 (1996).
[13] H. J. Zhai, L. S. Wang, A. E. Kuznetsov, and A. I. Boldyrev, J. Phys. Chem. A **106**, 5600 (2002).
[14] Z. Li, C. Zhao, and L. Chen, Theochem **854**, 46 (2008).
[15] L. Gao, P. Li, H. Lu, S. F. Li, and Z. X. Guo, J. Chem. Phys. **128**, 194304 (2008).
[16] J. M. Jia, G. B. Chen, D. N. Shi, and B. L. Wang, Eur. Phys. J. D **47**, 359 (2008).
[17] H. K. Yuan, H. Chen, A. L. Kuang, Y. Miao, and Z. H. Xiong, J. Chem. Phys. **128**, 094305 (2008).
[18] P. Weis, S. Gilb, P. Gerhardt, and M. M. Kappes, Int. J. Mass Spectrom. **216**, 59 (2002).
[19] T. G. Dietz, M. A. Duncan, D. E. Powers, and R. E. Smalley, J. Chem. Phys. **74**, 6511 (1981).
[20] P. Milani and W. A. deHeer, Rev. Sci. Instrum. **61**, 1835 (1990).
[21] U. Heiz, F. Vanolli, L. Trento, and W.-D. Schneider, Rev. Sci. Instrum. **68**, 1986 (1997).
[22] P. Weis, T. Bierweiler, E. Vollmer, and M. M. Kappes, J. Chem. Phys. **117**, 9293 (2002).
[23] See supplementary material at http://dx.doi.org/10.1063/1.3703014 for cartesian coordinates of all structures investigated as well as experimental and calculated molecular scattering functions for Bi_{11}^+-Bi_{14}^+ and arrival time distributions for Bi_9^+.
[24] A. A. Shvartsburg, B. Liu, M. F. Jarrold, and K.-M. Ho, J. Chem. Phys. **112**, 4517 (2000).
[25] D. Schooss, M. N. Blom, J. H. Parks, B. von Issendorff, H. Haberland, and M. M. Kappes, Nano Lett. **5**, 1972 (2005); M. N. Blom, D. Schooss, J. Stairs, and M. M. Kappes, J. Chem. Phys. **124**, 244308 (2006).
[26] H. Haberland, M. Mall, M. Moseler, Y. Qian, T. Reiners, and Y. Thurner, J. Vac. Sci. Technol. A **12**, 2925 (1994).
[27] Locally modified version of turbomole Version 6.3, (c) TURBOMOLE GmbH 2011. TURBOMOLE is a development of University of Karlsruhe and Forschungszentrum Karlsruhe 1989-2007, TURBOMOLE GmbH since 2007.
[28] J. Tao, J. P. Perdew, V. N. Staroverov, and G. E. Scuseria, Phys. Rev. Lett. **91**, 146401 (2003).
[29] K. Eichkorn, O. Treutler, H. Öhm, M. Häser, and R. Ahlrichs, Chem. Phys. Lett. **240**, 283 (1995); F. Weigend, Phys. Chem. Chem. Phys. **8**, 1057 (2006).
[30] B. Metz, H. Stoll, and M. Dolg, J. Chem. Phys. **113**, 2563 (2000).
[31] M. K. Armbruster, F. Weigend, C. van Wüllen, and W. Klopper, Phys. Chem. Chem. Phys. **10**, 1748–1756 (2008).
[32] D. M. Deaven and K. M. Ho, Phys. Rev. Lett. **75**, 288 (1995); M. Sierka, J. Döbler, J. Sauer, G. Santambrogio, M. Brümmer, L. Wöste, E. Janssens, G. Meijer, and K. R. Asmis, Angew. Chem., Int. Ed. **46**, 3372 (2007); M. Sierka, Prog. Surf. Sci. **85**, 398 (2010).
[33] F. Weigend and R. Ahlrichs, Phys. Chem. Chem. Phys. **7**, 3297 (2005).
[34] F. Weigend and A. Baldes, J. Chem. Phys. **133**, 174102 (2010).
[35] R. Kelting, R. Otterstätter, P. Weis, N. Drebov, R. Ahlrichs, and M. M. Kappes J. Chem. Phys. **134**, 024311 (2011).
[36] N. Drebov, E. Oger, T. Rapps, R. Kelting, D. Schooss, P. Weis, M. M. Kappes, and R. Ahlrichs, J. Chem. Phys. **133**, 224302 (2010).
[37] E. Oger, R. Kelting, P. Weis, A. Lechtken, D. Schooss, N. R. M. Crawford, R. Ahlrichs, and M. M. Kappes, J. Chem. Phys. **130**, 124305 (2009).
[38] D. Schooss, P. Weis, O. Hampe, and M. M. Kappes, Philos. Trans. R. Soc. London, Ser. A **368**, 1211 (2010).
[39] N. Wiberg, E. Wiberg, and A. F. Holleman, *Lehrbuch der Anorganischen Chemie*, 102th ed. (de Gruyter, Berlin, 2007).
[40] D. D. Wagman, W. Evans, V. B. Parker, R. H. Schumm, I. Halow, S. M. Bailey, K. L. Churney, and R. L. Nuttall, J. Phys. Chem. Ref. Data **11**(2), 2 (1982).
[41] A. Baldes, R. Gulde, and F. Weigend, J. Cluster Sci. **22**, 355 (2011).